

Cortactin Controls Surface Expression of the Voltage-gated Potassium Channel $K_V10.1$

Received for publication, April 16, 2012, and in revised form, October 22, 2012. Published, JBC Papers in Press, November 9, 2012, DOI 10.1074/jbc.M112.372540

Solveig Herrmann[‡], Milena Ninkovic^{§1}, Tobias Kohl^{§2}, Éva Lörinczi^{§3}, and Luis A. Pardo^{‡4}

From the [‡]Oncophysiology Group and [§]Department of Molecular Biology of Neuronal Signals, Max-Planck Institute of Experimental Medicine, Hermann-Rein-Str. 3, 37075 Göttingen, Germany

Background: $K_V10.1$ is a potassium channel expressed in the brain and important for non-neural tumorigenesis.

Results: An interaction between the C terminus of $K_V10.1$ and the proline-rich domain of cortactin stabilizes the channel at the plasma membrane.

Conclusion: Cortactin interacts with $K_V10.1$ and controls surface expression of the channel.

Significance: Our findings provide a functional and mechanistic link between the functions of two oncology-relevant proteins.

$K_V10.1$ is a voltage-gated potassium channel aberrantly expressed in many cases of cancer, and participates in cancer initiation and tumor progression. Its action as an oncoprotein can be inhibited by a functional monoclonal antibody, indicating a role for channels located at the plasma membrane, accessible to the antibody. Cortactin is an actin-interacting protein implicated in cytoskeletal architecture and often amplified in several types of cancer. In this study, we describe a physical and functional interaction between cortactin and $K_V10.1$. Binding of these two proteins occurs between the C terminus of $K_V10.1$ and the proline-rich domain of cortactin, regions targeted by many post-translational modifications. This interaction is specific for $K_V10.1$ and does not occur with $K_V10.2$. Cortactin controls the abundance of $K_V10.1$ at the plasma membrane and is required for functional expression of $K_V10.1$ channels.

Actin cytoskeleton remodeling is crucial for many cellular processes such as migration, invasion, endocytosis, or cell cycle progression. Cortactin (CTTN)⁵ therefore plays a central role in these processes, because it interacts with the cortical actin network and is able to alter it (see for example, Ref. 1). To fulfill this role, CTTN requires the interplay of several functional domains and different binding partners as well as post-translational modifications. CTTN binds F-actin through the actin binding repeats (1) and regulates its polymerization via binding and activation of the Arp2/3 complex at the CTTN N-terminal acidic domain (2, 3). This region is followed by an α -helical domain including a calpain cleavage site and a proline-rich

region, which harbors multiple tyrosine, threonine, and serine phosphorylation sites. Many kinases, including Src, are reported to act on these sites to control CTTN function in response to intracellular signaling cascades. Therefore, CTTN is thought to act as a key regulator transmitting kinase signaling toward actin remodeling (4). At its extreme C terminus, CTTN possesses a Src homology 3 domain (SH3), where binding of several interacting partners is observed, linking CTTN to several additional cell signaling pathways (1).

Lately, CTTN has been reported to affect the voltage-gated potassium channel $K_V1.2$ and the large conductance calcium- and voltage-activated potassium channel, $K_{Ca}1.1$ (BK, *KCNMA1*), by altering their surface expression or conducting properties, respectively (4–8). It has been proposed that these processes are due to a CTTN-mediated linkage of these ion channels with the cytoskeleton. At least for $K_V1.2$, this seems to be a phosphorylation-dependent process, which influences receptor-mediated endocytosis of this channel (5, 8).

The voltage-gated potassium channel $K_V10.1$ has attracted particular interest for its ability to transform cells and its resulting oncological relevance (9, 10). This behavior has been partially attributed to the role of $K_V10.1$ in cell cycle control downstream of p53 (11). Blocking $K_V10.1$ in MCF-7 cells arrests them in the G₁ phase of the cell cycle and inhibits expression of cell cycle-related genes such as cyclin D1 (*CCND1*) and E (*CCNE*) (11–13). On the other hand, $K_V10.1$ itself is regulated during the cell cycle and it shows altered conductive properties and reduced current in the M phase (14, 15). This regulation process is thought to be induced by alterations of the interaction of the ion channel with the cytoskeleton (15).

In this study, we identified CTTN as an interaction partner of $K_V10.1$ *in vivo* and confirmed this with different approaches. Our results clearly show that CTTN expression is essential for the surface expression of $K_V10.1$ and it dramatically influences the $K_V10.1$ -mediated current by regulating its membrane localization. Given that CTTN is often overexpressed in cancer (being part of the well described 11q3 amplicon (16)) and linked to tumor invasiveness (17), CTTN and $K_V10.1$ could have a synergistic effect on their transforming properties. CTTN might serve to connect $K_V10.1$ and central signaling pathways in the cell, for example, during the cell cycle.

⌘ Author's Choice—Final version full access.

¹ Present address: Dept. of Neurosurgery, Georg August University Medical Center, Göttingen, Germany.

² Present address: Dept. of Cardiology & Pneumology, Translational Cardiology, Georg August University Medical Center, Göttingen, Germany.

³ Present address: Dept. of Cell Physiology and Pharmacology, University of Leicester, Leicester, UK.

⁴ To whom correspondence should be addressed: AG Onkophysiologie, Max-Planck-Institut für experimentelle Medizin, Hermann-Rein-Str. 3, 37975 Göttingen, Germany. Tel.: 49-551-3899-646; Fax: 49-551-3899644; E-mail: pardo@em.mpg.de.

⁵ The abbreviations used are: CTTN, cortactin; SH3, Src homology 3; BBS, bungarotoxin-binding site; BTX, bungarotoxin; PTO, phosphorothioate antisense oligodeoxynucleotide; FAK, focal adhesion kinase; N-term, N-terminal.

Cortactin Controls $K_v10.1$ Functional Expression

EXPERIMENTAL PROCEDURES

Yeast Two-hybrid—The yeast reporter strain L40 (18) (*MATa, trp1, leu2, his3, LYS::lexA-HIS3, URA3::lexA-lacZ*) was transformed with pLexN- $K_v10.1$ by the lithium acetate method and grown on synthetic medium lacking tryptophan. Following further transformation with plasmid pVP16-3-cDNA (postnatal 8 rat brain cDNA library, kindly provided by Nils Brose), double transformants were plated on synthetic medium lacking histidine, leucine, uracil, lysine, and tryptophan and in the presence of the competitive inhibitor of the HIS3 protein 3-amino-1,2,4-triazole. Positive colonies were picked after 4–6 days and tested for β -galactosidase activity using the plate assay. Plasmids from positive clones were rescued and transformed in *Escherichia coli* strain HB101. *E. coli* cells were plated on leucine-lacking medium. Positive clones were further analyzed by yeast retransformation and DNA sequencing.

Expression and Purification of GST-tagged Proteins—Full-length CTTN (accession number NM 005231.3) or fragments N-term (residues 1–329), N-term-H (residues 1–400), HP (residues 360–495) and SH3 (residues 475–551) were cloned into pGEX-4T-1 (GE Healthcare) expression vector to introduce an N-terminal GST tag. Expression was performed in *E. coli* BL21(D3) after induction with 0.05 mM isopropyl 1-thio- β -D-galactopyranoside for 3 h at 37 °C. Cells were harvested and resuspended in 10 mM Tris-HCl (pH 8.0), 150 mM NaCl, 1 mM EDTA. After treatment with 0.1 mg/ml of lysozyme on ice, cells were sonicated (Sonotrode TT13). The soluble fraction was supplemented with protease inhibitors and used for further purification with glutathione-agarose beads (Sigma) according to the manufacturer's instructions. Quality and quantity of purified proteins was checked using SDS-PAGE.

Cell Culture and Transfection—HeLa cells were cultured in minimal essential medium + GlutaMax (Invitrogen) supplemented with 10% FCS (PAA), HEK293 cells in DMEM/F-12 + GlutaMax (Invitrogen) supplemented with 10% FCS and Zeocin (Cayla; 300 μ g/ml) in the case of the stable cell line HEK293/ $K_v10.1$ -BBS (HEK-BBS (19)) at 10% CO₂ and 37 °C. Proliferation was determined with alamarBlue as described previously (20).

Transfection was performed using Lipofectamine 2000 or Lipofectamine (Invitrogen) according to the manufacturer's instructions. Knockdown of CTTN was induced by transfection with siRNA against human CTTN (Dharmacon), "all stars" negative control siRNA (Qiagen) was used to control for off-target effects. For the expression of $K_v10.x$ -BBS and CTTN (with or without fusion to Venus), sequence coding for these proteins were cloned in pcDNA3 or pECFP-N1 vectors. Empty vectors were used as controls.

Fractional Labeling, Quantification, and Purification of $K_v10.1$ -BBS— $K_v10.1$ -BBS is a tagged $K_v10.1$ channel that carries the bungarotoxin-binding site from the acetylcholine receptor inserted in the extracellular loop between transmembrane segments 3 and 4 (19). Labeling of whole cell $K_v10.1$ -BBS was performed in cell lysates in buffer LP (20 mM Tris-HCl, pH 7.4, 150 mM NaCl, 5 mM MgCl₂, 1% Nonidet P-40, protease inhibitors (Roche Applied Science)) with α -bungarotoxin-biotin (α -BTX-biotin) conjugate (Invitrogen) at a final concentra-

tion of 0.2 μ g/ml for 30 min on ice. To detect membrane and/or internalized $K_v10.1$ -BBS, living cells (HEK-BBS) were incubated in media supplemented with α -BTX-biotin conjugate at a final concentration of 2.5 μ g/ml and kept at room temperature for 10 min (membrane) or at 37 °C for 1 h (internalized). For internalized $K_v10.1$ -BBS, cells were washed with ice-cold acid wash buffer (150 mM NaCl, pH 3.0) for 3 min to remove membrane labeling of $K_v10.1$ -BBS. Twice washing with cold PBS removed the residual α -BTX-biotin conjugate. Cells were then harvested and lysed with LP buffer for 20 min on ice. The insoluble fraction was removed by centrifugation at 18,000 \times g at 4 °C, and the supernatant was used for ELISA or pull-down experiments. $K_v10.1$ -BBS expressed in *Xenopus* oocytes injected with the corresponding cRNA was processed in the same way as that from HEK-BBS cells.

For pulldown approaches, labeled $K_v10.1$ -BBS was bound to streptavidin-coated magnetic beads (T1, Invitrogen) for at least 30 min at 4 °C. Unbound protein was removed by washing twice with a stringent series of four washing buffers (1, LP; 2, 1% dioxane, 0.5% Nonidet P-40, 300 mM NaCl, 50 mM Tris-HCl, pH 7.4, 5 mM EDTA; 3, 10% dioxane, 0.1% Nonidet P-40, 1 M NaCl, 50 mM Tris-HCl, pH 7.4, 5 mM EDTA; and 4, TBS).

Quantification of the amount of labeled $K_v10.1$ -BBS was performed by ELISA. After labeling, total cell lysates (30 and 150 μ g of protein), were immobilized on streptavidin-coated plates (Pierce) and detected using a C-terminal monoclonal anti- $K_v10.1$ antibody (Ab33, 5 μ g/ml) and a polyclonal anti-mouse secondary antibody (Pierce, 1:500) coupled to peroxidase. ABTS (Invitrogen) was used as a substrate for development and detected in a Wallac Victor2 reader at 405 nm (reference 490 nm). Experiments were performed in duplicate.

Pull-down Experiments—For immunoprecipitation, rat brain lysates (800 μ g of total protein) were incubated overnight at 4 °C with 2–5 μ g of antibody (anti- $K_v10.1$ 33/62 (21); anti-CTTN (Millipore); or nonspecific mouse IgG κ 2b) in buffer A (0.5% Triton X-100, 25 mM Tris-HCl, pH 7.5, 75 mM NaCl, 2.5 mM EDTA and protease inhibitors (Roche Applied Science)). Pull down was performed by adding 20 μ l of Protein G/A-coated Sepharose beads (Calbiochem) for 2 h at 4 °C under rotation. After washing five times with buffer A, bound protein was eluted at 70 °C for 10 min using LDS sample buffer containing reducing agent (Invitrogen) and analyzed by SDS-PAGE (Invitrogen) and Western blotting.

To test binding to CTTN (full-length or partial domains), the GST-tagged constructs were incubated with $K_v10.1$ -BBS immobilized on streptavidin-coated beads (Invitrogen), in PBS supplemented with protease inhibitors (Roche Applied Science) overnight at 4 °C. Unbound protein was washed away in five washing steps (PBS) before eluting specifically bound proteins by incubation at 70 °C for 10 min using LDS sample buffer containing reducing agent (Invitrogen). Eluted proteins were analyzed by SDS-PAGE (Invitrogen) and Western blotting.

All pull-down and immunoprecipitation experiments were performed at least three times independently with essentially identical results. The figures show representative examples.

Electrophysiology—Recordings on *Xenopus* oocytes were performed as described in Ref. 22 using a Turbo TEC-10CD amplifier (NPI electronics). cRNA was synthesized using the

mMessage mMachine kit (Ambion) according to the manufacturer's instructions. 0.1–1 ng of cRNA per oocyte were microinjected 1–3 days prior to recording. When not otherwise indicated, 5 ng of the phosphorothioate antisense oligodeoxynucleotide (PTO; CAGTCGCTGTCTCATCTG; Ref. 8) was injected to deplete CTTN. The sense oligodeoxynucleotide served as control. Cells were kept at 18 °C in ND 96 solution (96 mM NaCl, 2 mM KCl, 0.2 mM $CaCl_2$, 2 mM $MgCl_2$, 5 mM Hepes/NaOH, pH 7.5) supplemented with theophylline (0.5 mM) to avoid maturation of the oocytes. For voltage clamp recordings, pipettes had resistances ranging from 0.5 to 1.2 M Ω when filled with 2 M KCl. External solution (NFR) contained 115 mM NaCl, 2.5 mM KCl, 1.8 mM $CaCl_2$, 10 mM Hepes/NaOH (pH 7.2). Current was digitized at 5 kHz and filtered at 1 kHz. Where relevant, voltage pulse protocols are described in the figure legends. Current amplitudes were compared by non-paired Student's *t* test. *p* values below 0.05 were considered statistically significant. Asterisks in the figures indicate *p* values (*, *p* < 0.05; **, *p* < 0.01; ***, *p* < 0.005).

Non-stationary noise analysis was carried out using an EPC9 patch clamp amplifier (HEKA Electronics) in the outside-out configuration on macropatches of *Xenopus* oocytes (23). Intracellular solution contained 100 mM KCl, 10 mM EGTA, 10 mM Hepes/KOH (pH 7.2). NFR was used as external measuring solution. Patches were held at a holding potential of –80 mV. Average currents were determined from at least 300 consecutive identical test pulses to +40 mV, and variance was calculated with PulseTools software (HEKA Electronics). Number of channels (*N*) and single channel currents (*i*) were determined from the variance (σ^2) versus amplitude (*I*) plot using Equation 1,

$$\sigma^2 - \sigma_0^2 = i \cdot I - \frac{I^2}{N} \quad (\text{Eq. 1})$$

where σ_0^2 represents the baseline variance (23).

Data acquisition and analysis was performed with PulseFit, PulseTools (HEKA Electronics), and IgorPro (WaveMetrics). All experiments were performed on oocytes from at least two different animals. The number of individual recordings is indicated in the figures.

Microscopy—HEK293 cells were plated in Nunc chambers (LabTek Chamber Slides 177399) and transfected with BBS-tagged constructs of $K_V10.x$ using Lipofectamine 2000 (Invitrogen). Labeling was performed 24 h after transfection for 1 h at 37 °C by adding Alexa Fluor 555-BTX conjugate (2 μ g/ml, Invitrogen) to the culture medium. After five washing steps with ice-cold PBS, live cell imaging was performed on a Zeiss Axiovert 200M microscope.

For confocal microscopy, HeLa cells were grown on glass coverslips, transfected, and fixed 24 h after transfection in 4% paraformaldehyde in PBS for 10 min at room temperature. Permeabilization was performed using 0.1% Triton X-100 in PBS for 10 min at room temperature. Nonspecific binding sites were blocked with 0.5% gelatin in PBS for 30 min at room temperature. To visualize $K_V10.x$ -BBS, permeabilized cells were treated with Alexa 555-BTX conjugate (0.5 μ g/ml, Invitrogen) for 1 h, washed thoroughly with PBS, and mounted with ProLong Gold Antifade Reagent (Invitrogen). To detect focal adhesion kinase

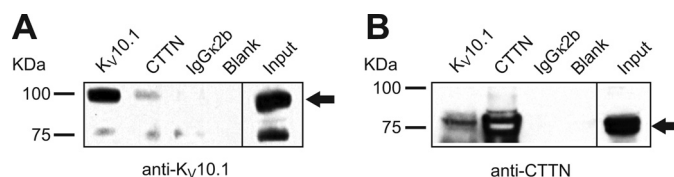


FIGURE 1. Co-immunoprecipitation of $K_V10.1$ and CTTN from rat brain lysates. Protein extract from rat brain was subjected to immunoprecipitation using Sepharose-linked antibodies against $K_V10.1$ (Ab 62/33), CTTN or isotype control IgG (*IgGκ2b*). Protein A/G-Sepharose beads alone served as an additional negative control (*blank*). The immunoprecipitated materials were then analyzed subsequently by SDS-PAGE and immunoblotting with either (A) rabbit anti- $K_V10.1$ or (B) mouse anti-CTTN antibodies.

(FAK) a mouse anti-FAK (BD Biosciences) antibody was used according to the manufacturer's instructions, with a secondary antibody conjugated to Alexa Fluor 555 (Invitrogen). Image acquisition was performed using a Zeiss LSM 510 Meta confocal microscope, and analysis was carried out with Fiji.

RESULTS

$K_V10.1$ and CTTN Interact Directly *In Vitro* via the Proline-rich Region of CTTN—To identify interacting partners of $K_V10.1$, we performed yeast two-hybrid screens using a rat brain expression library. Full-length $K_V10.1$ fused to the DNA binding domain of the bacterial LexA transcription factor was used as bait to screen a rat brain cDNA library fused to the activation domain of the VP16 transcription factor. Of 2 million screened clones, eight were positive for the *HIS3* marker. After sequencing, one of the clones was found to contain the coding sequence for CTTN. Co-immunoprecipitation studies on native tissue confirmed the interaction of $K_V10.1$ and CTTN. Immunoprecipitation of $K_V10.1$ co-precipitated CTTN and, in the converse experiment, antibodies against CTTN precipitated $K_V10.1$ from rat brain lysates, indicating that physical interaction between CTTN and $K_V10.1$ occurs *in vivo* (Fig. 1).

To study the determinants for interaction, we generated tagged proteins for pull-down assays: an N-terminal GST-CTTN fusion protein (purified from bacteria) and an BTX-binding site (BBS)-labeled $K_V10.1$. The labeled $K_V10.1$ construct was generated by inserting BBS between transmembrane segments 3 and 4. This construct has been confirmed to elicit currents similar to wild-type $K_V10.1$ and been exposed to the extracellular milieu (19). $K_V10.1$ -BBS was stably expressed in HEK 293 cells and pulled down using streptavidin-coated beads. The resulting purified $K_V10.1$ was able to precipitate the GST-CTTN fusion protein (Fig. 2A) but not GST alone (Fig. 2B), confirming the interaction between these two tagged proteins. In this type of experiment, we also observed some co-precipitation when using $K_V10.2$, the closest relative to $K_V10.1$, but the specific signal was much weaker (Fig. 2A).

To narrow down the region responsible for mediating the interaction between these proteins, we constructed fragments of CTTN based on the functional domains described for this protein: the N-terminal acidic domain and the neighboring actin binding repeats responsible for actin binding and polymerization, and the proline-rich region, which is flanked by a helical and a classical SH3 domain (1). Thus, we designed four CTTN fragments (Fig. 2C): -N-term (residues 1–329), spanning the N-terminal acidic domain and the actin repeats; -N-term-H

Cortactin Controls $K_V10.1$ Functional Expression

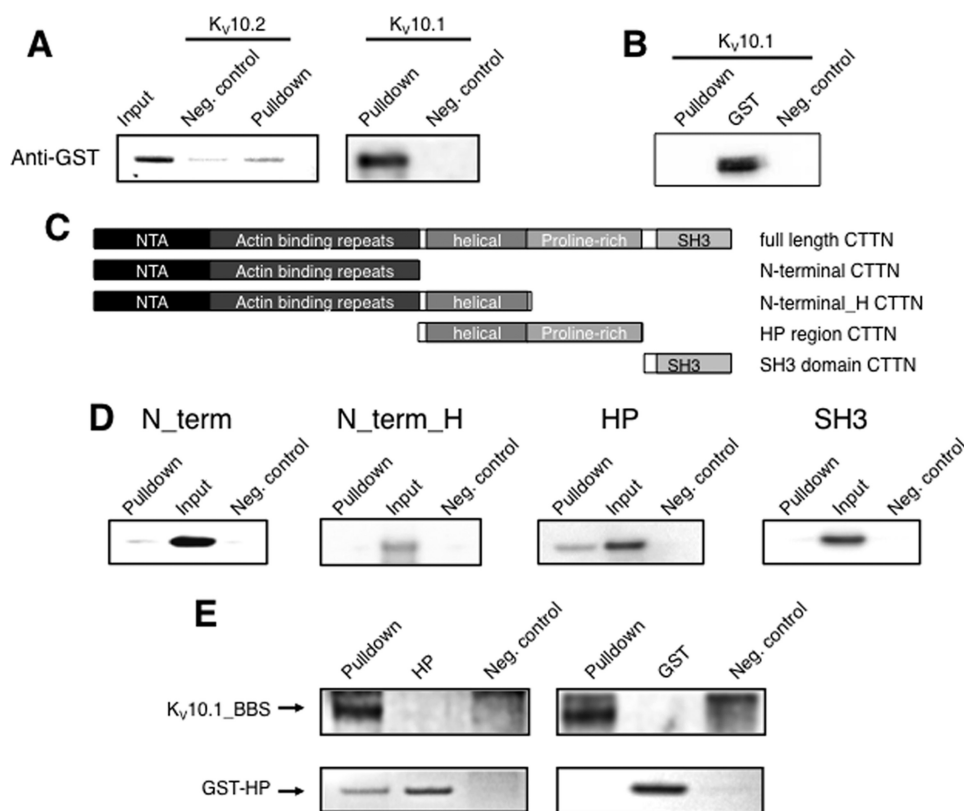


FIGURE 2. $K_V10.1$ is able to pull down CTTN *in vitro*. $K_V10.1$ -BBS or $K_V10.2$ -BBS were labeled with BTX-biotin (+Bb) in lysates of HEK293 cells expressing either $K_V10.1$ -BBS or $K_V10.2$ -BBS, pulled down, and washed rigorously using streptavidin-coated beads. The streptavidin-precipitated proteins were then used in pull-down experiments with various GST-CTTN fusion proteins that were then analyzed by SDS-PAGE followed by immunoblotting using an anti-GST antibody (Santa Cruz Biotechnology) (A, B, and D) or Coomassie staining (E). Unlabeled cell lysates served as a negative control (–Bb). Both $K_V10.1$ and $K_V10.2$ were able to precipitate the full-length GST-CTTN (A) but not GST alone (B). C, Schematic representation of the various CTTN domain GST-tagged proteins using pull-down assays with $K_V10.1$ -BBS. Of these CTTN domain containing fusions only the HP region was precipitated by $K_V10.1$ -BBS (D). Specific pull down of GST-HP-region of CTTN by $K_V10.1$ was also confirmed in Coomassie stained gels (E).

(residues 1–400), which adds the helical region to N-term; -HP (residues 360–495), corresponding to the helical and proline-rich regions; and -SH3 (residues 475–551), namely the classical SH3 domain of CTTN.

Three of these constructs (N-term, HP, and SH3) were cloned in the pLexN vector and tested in the yeast two-hybrid system for interaction with $K_V10.1$ domains in pVP16–4: N terminus, (residues 1–220), C terminus, (residues 478–963), or full-length $K_V10.1$. We did not detect interactions with the N-term or HP constructs. In this approach, the SH3 domain could not be evaluated because it showed autoactivation activity.

We then tested the ability of $K_V10.1$ to pull down the purified GST-tagged CTTN domains. Only GST-HP clearly showed interaction to $K_V10.1$, whereas no or only a very weak signal was detected in GST-N-term, GST-N-term-H, or GST-SH3 pull-down (Fig. 2D). We were also able to detect binding of the HP region to $K_V10.1$ in a large scale pull-down followed by Coomassie stain (Fig. 2E). This result strongly suggests that the interaction between $K_V10.1$ and CTTN interaction occurs through the proline-rich region of CTTN.

CTTN Influences $K_V10.1$ -mediated Current—Having established that CTTN and $K_V10.1$ interact directly, we asked next if there is a functional consequence associated with this interaction. CTTN is known to regulate the current through $K_V2.1$ (by altering its surface expression (5, 8)) and $K_{Ca}1.1$ (BK, by chang-

ing its interaction with the actin cytoskeletal and thereby the open probability of the channel (6, 7)).

To test whether the $K_V10.1$ current was affected, we manipulated the levels of CTTN in *Xenopus laevis* oocytes expressing $K_V10.1$. To increase CTTN levels, we injected cRNA encoding human CTTN; to reduce the endogenous CTTN, we injected a specific PTO previously reported to deplete CTTN (8). We then measured the current mediated by $K_V10.1$ channels.

In these experiments, the macroscopic $K_V10.1$ current amplitude depended on the presence of CTTN, but $K_V10.1$ currents in CTTN-depleted or overexpressing oocytes did not differ in kinetics or voltage dependence from those obtained in untreated oocytes. $K_V10.1$ produced slowly activating, outward rectifying currents, which did not inactivate; a slight inward rectification was observed with strong depolarizations compatible with block by intracellular sodium (14) (Fig. 3A). The current-voltage relationships were also unchanged by CTTN depletion or overexpression (Fig. 3B). A defining feature of the $K_V10.1$ current is the dependence of the time constant of activation on the holding potential in such a way that the current activates slower the more negative the prepulse potential (24). This property was also not affected by CTTN depletion or overexpression (Fig. 3C).

Depletion of CTTN by PTO injection reduced or even abolished the $K_V10.1$ current in a dose-dependent manner (Fig. 3D). We subsequently used injections of 5 ng of PTO per oocyte as a

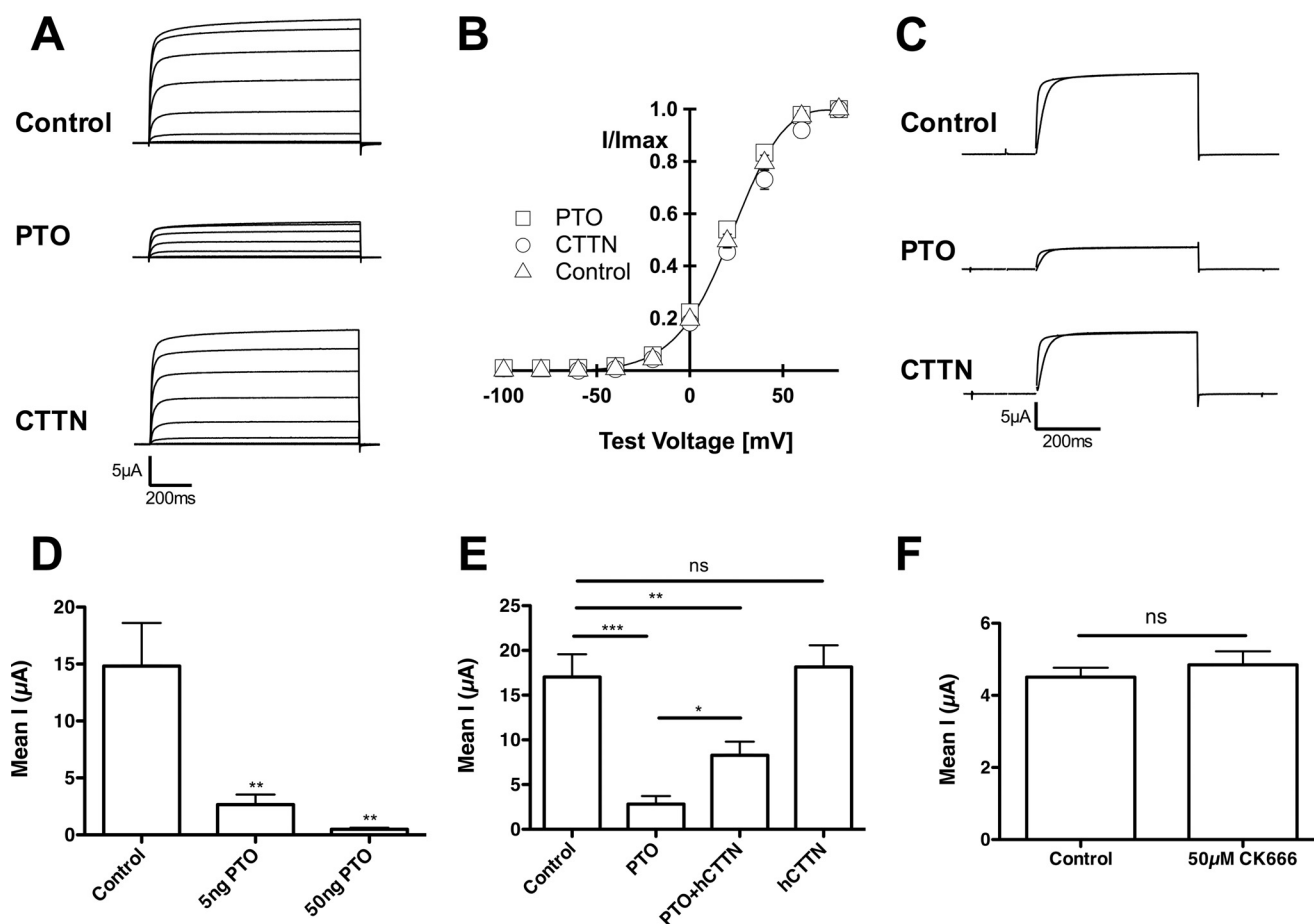


FIGURE 3. Effect of CTTN depletion and overexpression on $K_v10.1$ -mediated current. Representative current traces of $K_v10.1$ expressed in *Xenopus* oocytes under control conditions (Control), depleted (PTO; via injection of an antisense oligonucleotide) or increased (CTTN; via overexpression) CTTN levels are shown. Test pulses were applied ranging from the holding potential of -100 to $+80$ mV in 20-mV increments evoked whole cell currents. To determine the current-voltage relationship, the steady state current (I) was measured at the end of each pulse and normalized to the recorded current at $+80$ mV (I_{max}). Increased or decreased levels of CTTN (PTO or CTTN, respectively) do not have any effect on the general characteristic current appearance (A) or on current-voltage relationships (B). C, $K_v10.1$ currents were evoked with a test pulse to $+40$ mV starting from either a holding potential of -100 or -70 mV. As expected for $K_v10.1$, the activation of current depended on the prepulse potential independent of CTTN expression levels. D and E, depletion of CTTN (PTO) significantly decreased current amplitudes at a test pulse of $+80$ mV in comparison to control levels. This effect was dependent on the amount of PTO injected (D). Overexpression of human CTTN was not able to increase current amplitudes over control levels significantly, but partially restored current amplitudes in PTO injected oocytes (E). F, incubation for 24 h with the Arp2/3 inhibitor CK-666 ($50 \mu\text{M}$) did not alter the current amplitude in oocytes expressing $K_v10.1$. Current amplitude was determined at the end of a depolarization to $+60$ mV.

working concentration because it led to a current reduction of more than 80% (to $18 \pm 6\%$) but still allowed quantification of the remaining current ($n = 12$, $p \leq 0.0001$, Fig. 3D). A similar behavior was observed when HEK293 cells expressing $K_v10.1$ were treated with siRNA against CTTN. $K_v10.1$ was measured in randomly chosen cells of each group, and the mean current density (pA/pF) was determined. Although the overall current values were not significantly different (210 ± 36 pA/pF in the controls and 179 ± 33 pA/pF in the siRNA-treated cells, $p = 0.5$), 11 of 28 treated cells (40%) showed current densities below 50 pA/pF, versus 4/23 (17%) in the controls, compatible with the expectation of an effect on current density only in a subset of cells successfully transfected with siRNA.

Increasing CTTN over physiological levels did not further enhance $K_v10.1$ -mediated currents ($117 \pm 16\%$, $n = 11$, $p = 0.6$, Fig. 3E). This was not due to a saturation of the translation/processing systems of the oocyte, as injection of larger amounts of $K_v10.1$ cRNA leads to an increase in current amplitudes (not shown). PTO does not hybridize to human CTTN (the best

match spans only 8 bases). Therefore, co-injection of the human cRNA should be able to replace the depleted CTTN of oocytes. This replacement restored $K_v10.1$ current amplitudes to $60 \pm 10\%$, $n = 17$ (Fig. 3E).

As CTTN is known to play important roles in cytoskeletal organization, it is possible that the effects observed are the result of interference rather than a direct effect on $K_v10.1$. To test this, we used the Arp2/3 complex inhibitor CK666 (25). $K_v10.1$ current amplitude was determined in oocytes incubated with $50 \mu\text{M}$ CK666 over 24 h (the entire incubation period after RNA injection). No differences were observed as compared with oocytes treated with vehicle (Fig. 3F), indicating that the effect of CTTN knockdown is independent of its role as an Arp2/3 activator. Taken together, these observations strongly indicate that CTTN regulates the amplitude of $K_v10.1$ -mediated currents.

Regulation by CTTN Is Specific to $K_v10.1$ and Depends on Its C Terminus—As $K_v10.2$ was able to bind CTTN in *in vitro* pull-down assays (Fig. 2B), we next examined the possible func-

Cortactin Controls $K_v10.1$ Functional Expression

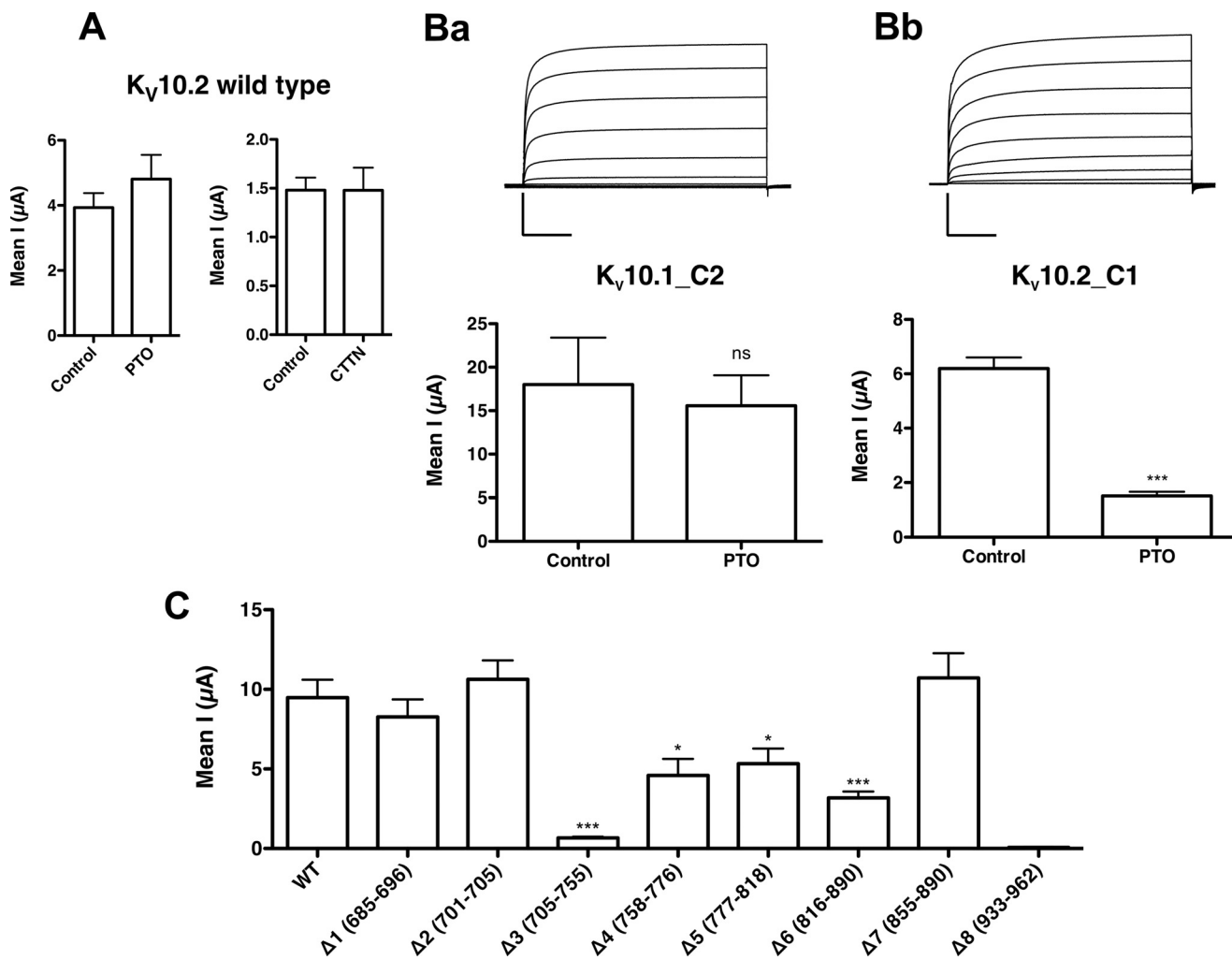


FIGURE 4. Regulating effect of the CTTN expression level depends on C terminus of $K_v10.1$. *A*, varying CTTN levels by depletion (PTO, left panel) or overexpression (CTTN, right panel) in *Xenopus* oocytes did not influence whole cell current amplitudes of $K_v10.2$ in comparison to control levels. *B*, exchanging C termini between $K_v10.1$ and $K_v10.2$ transfers current dependence to CTTN levels. Current amplitudes of $K_v10.1$ bearing the $K_v10.2$ C terminus (*B*, panel *a*) were no longer sensitive to CTTN depletion in contrast to currents mediated by $K_v10.2$ bearing the $K_v10.1$ C terminus (*B*, panel *b*), which were significantly affected by CTTN reduction with injection of PTO. Current traces above the bar diagrams show typical responses elicited by the respective chimeras in *Xenopus* oocytes (see legend to Fig. 3). Scale bars: 5 μ A, 200 ms. *C*, effect of partial deletion of the $K_v10.1$ C terminus on current amplitudes. Partial deletions of the C terminus of $K_v10.1$ were generated and expressed in *Xenopus* oocytes. Current amplitudes of deletions $K_v10.1$ $\Delta 3$, $\Delta 4$, $\Delta 5$, $\Delta 6$, and $\Delta 8$ were significantly reduced compared with the wild type.

tional effects of CTTN depletion on $K_v10.2$ currents in *Xenopus* oocytes. We found that currents evoked by this channel were not significantly affected by depletion of CTTN levels ($133 \pm 21\%$ of control levels, $n = 30$, $p = 0.2$; Fig. 4*A*). Overexpression of CTTN also did not have an effect on $K_v10.2$ -mediated currents ($100 \pm 17\%$ of control levels, $n = 10$, $p = 0.99$; Fig. 4*A*). The kinetic properties of the macroscopic currents of $K_v10.2$ were also unaffected.

Although both channels are very similar in sequence and structure, they differ widely in their expression patterns and functions (26–28) and it is formally possible that they are regulated by different mechanisms. $K_v10.1$ and $K_v10.2$ share high sequence homology and the differences between them are concentrated in the C terminus, so we next tested the effect of CTTN depletion on K_v10 chimeras with exchanged C termini. Both chimeric channels expressed in *Xenopus* oocytes were functional, showing robust currents (Fig. 4*B*) with kinetics and voltage dependence very similar to wild-type currents. Current

amplitudes of $K_v10.1$ bearing the C terminus of $K_v10.2$ were no longer sensitive to CTTN depletion ($145 \pm 15\%$ of control levels, $n = 23$, $p = 0.11$), whereas those of $K_v10.2$ with the C terminus of $K_v10.1$ showed a prominent reduction upon PTO injection ($22 \pm 3\%$ of control levels, $n = 16$, $p < 0.0005$, Fig. 4*B*). This supports the idea that the C terminus of $K_v10.1$ mediates the functional interaction of $K_v10.1$ and CTTN.

To further map the binding site of CTTN within the C terminus of $K_v10.1$, we constructed mutated channels with various C-terminal deletions ($K_v10.1$ $\Delta 1$ – $\Delta 8$, Fig. 4*C*). Deletions were chosen in those regions that differ most between $K_v10.1$ and $K_v10.2$. As depletion of endogenous CTTN greatly reduced the $K_v10.1$ -mediated current, we expected the deletion of the CTTN binding site to have the same effect. Indeed, we found that five of the eight deletion mutants produced reduced current amplitudes (Fig. 4*C*). One group of deletions, namely $K_v10.1$ $\Delta 4$ – $\Delta 6$ showed only moderate reduction of current amplitude, which was further decreased by depletion of CTTN

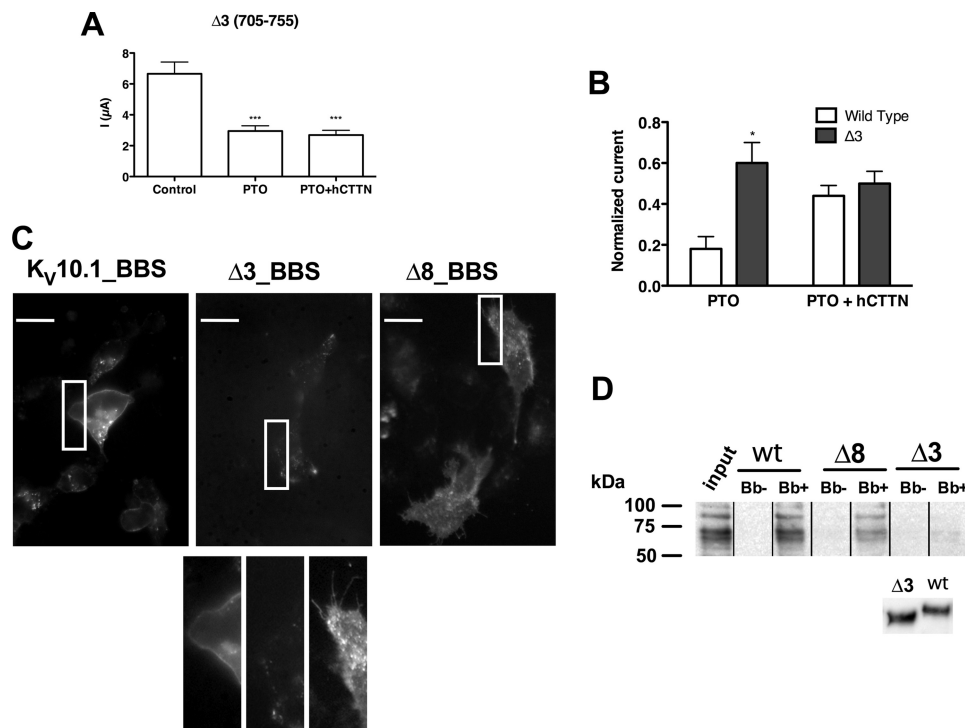


FIGURE 5. Deleting amino acids 705–755 of $K_v10.1$ changes its distribution as well as its ability to bind CTTN. *A*, depletion of CTTN by co-injection of the PTO oligonucleotide was able to reduce current amplitudes of $K_v10.1$ $\Delta 3$ (del705–755) in voltage clamp oocyte recordings as determined by a depolarization step to +80 mV. Restoration of CTTN levels by injection of human CTTN did not rescue the effect of PTO on this mutant. *B*, the effect of PTO-mediated CTTN depletion on $K_v10.1$ $\Delta 3$ was weaker (reducing current amplitude by 50%) than that observed in full-length $K_v10.1$ (that reduced current by 80%). Current amplitude of the mutant $K_v10.1$ $\Delta 3$ after CTTN depletion was not rescued by additional expression of human CTTN, in contrast to wild-type $K_v10.1$. *C*, membrane $K_v10.1$ -BBS was labeled using a BTX-Alexa 555 conjugate and allowed for internalization for 1 h. Washed cells were analyzed by wide field microscopy. $K_v10.1$ -BBS as well as $K_v10.1$ -BBS $\Delta 8$ (del933–962) showed prominent membranous labeling of $K_v10.1$ -BBS, whereas nearly no membrane-bound $K_v10.1$ -BBS $\Delta 3$ was observed. Scale bar, 10 μm . *D*, $K_v10.1$ -BBS and $K_v10.1$ -BBS $\Delta 8$ successfully precipitated GST-CTTN, $K_v10.1$ -BBS $\Delta 3$ showed much weaker co-precipitation of the full-length CTTN. Mutants $K_v10.1$ -BBS $\Delta 3$, $K_v10.1$ -BBS $\Delta 8$, or wild-type $K_v10.1$ -BBS were transiently expressed in HEK 293 cells. Lysates were labeled with BTX-biotin (Bb) to pull down $K_v10.1$ -BBS using streptavidin-coated beads, unlabeled lysates served as negative control. Subsequent GST-CTTN was added and analyzed for co-precipitation using SDS-PAGE followed by Western blotting using a GST antibody.

(not shown). This indicates that these regions are not implicated in the $K_v10.1$ -CTTN interaction. Deletion of amino acid residues 705–755 ($K_v10.1$ $\Delta 3$) or the extreme C terminus ($K_v10.1$ $\Delta 8$) led to a reduction of current amplitudes by more than 90% (Fig. 4C), so we concentrated on these two constructs for further analysis.

To check if depletion of CTTN has any effect on current amplitudes of the mutants we increased the amount of cRNA injected to obtain quantifiable currents, and then measured the effect of CTTN knockdown on current amplitudes in experiments equivalent to those performed on wild-type channels (Fig. 1E). Current amplitudes for $K_v10.1$ $\Delta 3$ were reduced to $49 \pm 8\%$ ($n = 19$, $p < 0.001$) by co-injection of the PTO (Fig. 5A). However, the effect of PTO injection was significantly weaker than in wild-type $K_v10.1$ (Fig. 5B). Restoration of CTTN expression levels by co-injection of human CTTN could not rescue current amplitudes of this mutant ($52 \pm 9\%$, $n = 15$, $p < 0.001$; Fig. 5, A and B). We were not able to record any currents for $K_v10.1$ $\Delta 8$, as reported previously (29) unless we used RNA concentrations in the range of 5000 times greater than those used for wild-type, and then only in very few cells.

A reduction of current amplitude can be due to a change in the electrophysiological properties of $K_v10.1$, or in the number of available channels at the surface. To distinguish between these two possibilities, we measured the expression at the

plasma membrane in a cell culture system by adding the BBS tag to the deletion mutants. Living HEK 293 cells expressing $K_v10.1$ -BBS, $K_v10.1$ $\Delta 3$ -BBS, or $K_v10.1$ $\Delta 8$ -BBS were labeled with a BTX-Alexa Fluor conjugate to visualize membrane and internalized $K_v10.1$ (19). A clear membrane staining as well as internalized $K_v10.1$ was seen independently of the presence of the extreme C terminus of $K_v10.1$ (Fig. 5C, $K_v10.1$ -BBS and $K_v10.1$ $\Delta 8$ -BBS). Despite robust expression levels of all three constructs, only $K_v10.1$ $\Delta 3$ -BBS showed reduced labeling; internalized $K_v10.1$ was stained, but there was minimal signal at the membrane (Fig. 5C). With our experimental protocol, only surface BBS can be detected. Therefore, there is probably a population of channels at the surface, but we were not able to detect it. Close-ups of the regions indicated by a white rectangle are shown in the lower panel. Peripheral staining was prominent in $K_v10.1$ -BBS, whereas only punctate structures could be detected in $K_v10.1$ $\Delta 3$ -BBS. $K_v10.1$ $\Delta 8$ -BBS showed an intermediate profile with clear staining of cellular processes, compatible with plasma membrane together with abundant punctate staining.

Precipitation studies with GST-CTTN using $K_v10.1$ -BBS $\Delta 3$ or $\Delta 8$, as described above, revealed that $K_v10.1$ $\Delta 8$ is able to bind GST-CTTN with an efficiency comparable with wild-type $K_v10.1$, whereas $K_v10.1$ $\Delta 3$ showed reduced binding capability (Fig. 5D), although co-precipitation of the HP-region of CTTN

Cortactin Controls $K_V10.1$ Functional Expression

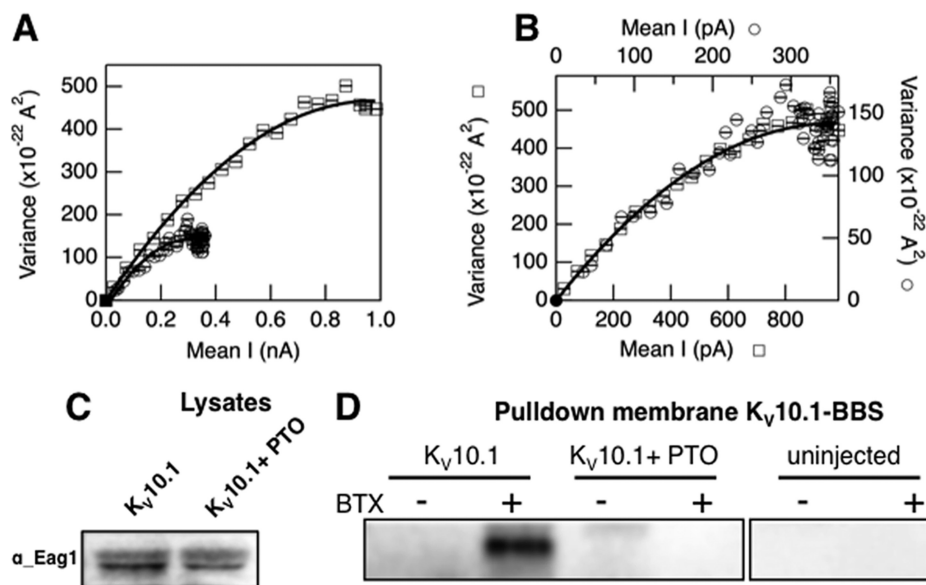


FIGURE 6. CTTN influences surface expression of $K_V10.1$. *A*, non-stationary noise analysis of $K_V10.1$ -mediated current in control and CTTN-depleted *Xenopus* oocytes. Representative plots of the variance against the mean current with the corresponding fitting parabola for patches derived from control untreated (squares) or CTTN-depleted (circles) oocytes. The same plots are shown with independent scales in the inset. The slope of the initial segment of the function (representing single channel current) did not change upon CTTN depletion. *B*, depletion of CTTN reduced surface levels of $K_V10.1$. Expression of $K_V10.1$ in *Xenopus* oocytes was analyzed by Western blot (WB) using anti- $K_V10.1$ antibodies. No difference of $K_V10.1$ expression was found in whole oocyte lysates in response to CTTN depletion with the PTO (left panel), whereas surface levels of $K_V10.1$ obtained from pull-down assays of membrane bound $K_V10.1$ -BBS were clearly reduced in the presence of the PTO (right panel).

was observed for $K_V10.1 \Delta 3$ (not shown). We therefore conclude that amino acid residues 705–755 of $K_V10.1$ contribute to the functional interaction with CTTN, but it is likely that other unidentified regions also participate in CTTN binding.

CTTN Does Not Influence the Biophysical Properties of $K_V10.1$ —Total current through an ion channel results from the combination of three parameters: the unitary current through a single channel (i), the total number of available channels (N), and the probability of a channel being open (P_o).

$$I = iNP_o \quad (\text{Eq. 2})$$

Thus, a change in I can be caused by altering channel surface expression (varying N) or eliciting a change in single channel conductance or open probability. Each of these possibilities is conceivable in the case of CTTN and $K_V10.1$. The cytoskeleton is known to play an important role in regulating the $K_V10.1$ -mediated current (15) and CTTN is reportedly involved in the regulation of the surface expression of some ion channels and receptors (8, 30); it can also alter the conducting properties of $K_{Ca}1.1$ channels by regulating its interactions with the actin cytoskeleton (6, 7). To distinguish between these possibilities, we used electrophysiological and biochemical techniques.

To determine electrophysiologically which of the above parameters is altered, we used non-stationary noise analysis, a technique that allows an estimation of I , N , and P_o from macroscopic currents based on the variance observed in the current trace. Variance is minimal both when all channels are either closed or open (see “Experimental Procedures”). We performed such analysis on excised *Xenopus* oocyte macropatches in the outside-out configuration. We averaged 300 depolarizing stimuli and determined point by point the variance of each trace with respect to the average trace. Fitting a parabola function

(Equation 1) to the current *versus* the variance data, the slope of the initial, pseudolinear segment of the distribution corresponds to the single channel current (23). The result of the fitting gave similar single channel currents in the presence (884 ± 64 fA) and absence (789 ± 68 fA, $p = 0.4$) of CTTN (Fig. 6A). When normalized to compensate for the smaller currents in patches from PTO-treated oocytes, the variance *versus* current plots overlapped (Fig. 6A, inset). Under the experimental conditions, the maximal open probability reached was similar in the presence or absence of CTTN (0.58 ± 0.03 *versus* 0.57 ± 0.04 , $p = 0.4$; Fig. 6C). Therefore, the parameter that is most likely influenced by CTTN knockdown is the number of available channels. These data strengthen the idea that CTTN influences the number of functional $K_V10.1$ channels at the plasma membrane.

Surface Expression of $K_V10.1$ Depends on the Presence of CTTN—We next analyzed the expression levels of $K_V10.1$ at the plasma membrane with biochemical techniques. Insertion of a BBS at the extracellular part of $K_V10.1$ allows specific labeling of membranous $K_V10.1$ -BBS in intact cells (19); cRNA encoding these modified proteins was injected into oocytes. Exposed $K_V10.1$ -BBS was labeled in the intact oocyte with BTX-biotin. Oocytes were then lysed, and labeled $K_V10.1$ -BBS was pulled down using streptavidin. In agreement with the electrophysiological data, CTTN-depleted cells showed a clear reduction in labeled $K_V10.1$ -BBS, indicating less protein at the cell surface in three independent experiments (Fig. 6B). Importantly, the total protein level of $K_V10.1$ in whole oocyte lysates was independent of CTTN levels (Fig. 6B, right panel), arguing against the possibility of reduced surface expression due to a reduction in the protein in the cell. Taken together, these

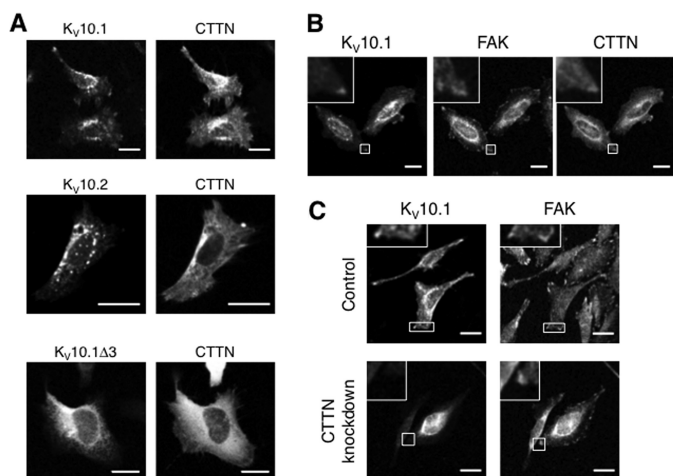


FIGURE 7. CTTN and $K_v10.1$ co-localize *in vivo*. *A*, transiently transfected HeLa cells were analyzed for the co-localization of CFP-CTTN with different $K_v10.x$ -BBS constructs by confocal microscopy. $K_v10.x$ -BBS constructs were visualized by labeling with a BTX-Alexa fluorophore after fixation and permeabilization of the cells. $K_v10.1$ -BBS showed typical distribution in the cells, co-localizing with CFP-CTTN mostly at the periphery of the cell (arrows). $K_v10.2$ -BBS as well as $K_v10.1 \Delta 3$ -BBS did not co-localize with CFP-CTTN, both having a completely different distribution compared with $K_v10.1$ -BBS. Deletion of amino acids 705–755 ($K_v10.1 \Delta 3$ -BBS) dramatically changed the intracellular localization of $K_v10.1$ to a diffuse staining mainly around the nucleus. *B*, co-staining with FAK revealed that the interaction between Venus-tagged $K_v10.1$ and CFP-CTTN occurs preferentially at focal adhesions. *C*, the cellular localization of $K_v10.1$ depends on the presence of CTTN. CTTN levels were manipulated in HeLa cells by siRNA-mediated knockdown or overexpression of CFP-CTTN. Fluorescent Venus-tagged $K_v10.1$ was expressed in these cells and analyzed for its cellular distribution using confocal microscopy. Control cells and cells overexpressing CTTN showed enrichment of the $K_v10.1$ signal in focal adhesions. This distribution was lost upon CTTN knockdown. Scale bars, 20 μ m.

results strongly suggest that CTTN regulates surface expression of $K_v10.1$ in *Xenopus* oocytes.

We then asked if observations made in oocytes could be translated to mammalian expression systems more suitable for studying trafficking processes. For this purpose, we first examined if alterations in CTTN expression levels induce changes in the cellular localization of $K_v10.1$ in mammalian cells. Cells with normal, reduced, or increased levels of CTTN were transfected with a fluorescent $K_v10.1$ -Venus fusion protein and analyzed by confocal microscopy. Overexpression of a CFP-tagged CTTN showed good co-localization with $K_v10.1$ -Venus throughout the cell (Fig. 7; thresholded Manders coefficient; tM, 0.73 ± 0.02) and at the membrane, especially at locations compatible with focal adhesions (tM, 0.77 ± 0.01).

Co-staining for FAK showed that co-localization between $K_v10.1$ and CTTN occurs at focal adhesions (Fig. 7). Co-localization of $K_v10.1$ -Venus and FAK can also be observed in cells with endogenous levels of CTTN (Fig. 7*B*). Depletion of CTTN by siRNA clearly changed the localization of $K_v10.1$; it was essentially absent from the cell margins, but there was a diffuse staining mainly around the cell nucleus. This manipulation also abolished the co-localization with FAK (Fig. 7*C*).

Depletion of CTTN had a very similar effect to deletion of amino acids 705–755 in the $K_v10.1$ C terminus ($K_v10.1 \Delta 3$ -BBS, Fig. 7*A*). CFP-CTTN showed weak co-localization with $K_v10.1 \Delta 3$ -BBS (tM, 0.29 ± 0.03 , Table 1) or $K_v10.2$ -BBS (tM, 0.31 ± 0.09). At the membrane or presumptive focal adhe-

TABLE 1
Quantification of co-localization with CTTN

	Location	Thresholded Manders coefficient	
		1	2
$K_v10.1$	Whole cell	0.75 ± 0.02 (87)	0.71 ± 0.02 (87)
	Adhesions	0.78 ± 0.01 (79)	0.76 ± 0.01 (79)
$K_v10.2$	Whole cell	0.32 ± 0.09 (12)	0.29 ± 0.07 (12)
	Adhesions	0.23 ± 0.02 (35)	0.23 ± 0.03 (35)
$K_v10.1 \Delta 3$	Whole cell	0.26 ± 0.05 (17)	0.31 ± 0.06 (17)
	Adhesions	0.27 ± 0.03 (40)	0.24 ± 0.03 (40)

sions, no co-localization of these two proteins was observed (Fig. 7*A*), again indicating that CTTN interacts with neither $K_v10.2$ nor $K_v10.1 \Delta 3$ -BBS *in vivo*.

We also labeled and tracked $K_v10.1$ -BBS in living cells using fluorescently labeled BTX. HEK 293 cells stably expressing $K_v10.1$ -BBS were transfected either with control (scrRNA) or siRNA directed against CTTN. Reduced CTTN levels to about 50% (as revealed by Western blot analysis, Fig. 8*A*) lowered surface staining by BTX (Fig. 8*B*). To quantify this effect, we performed ELISA on BTX-coated plates (by immobilization of BTX-biotin on streptavidin-coated plates). Labeled cell extracts were incubated on these plates and $K_v10.1$ was detected using a C-terminal antibody. Different labeling protocols enabled us to distinguish between different fractions of $K_v10.1$ -BBS. Incubating with BTX after cell lysis labels total $K_v10.1$ and not just the exposed fraction. Quantification showed that changing the CTTN expression levels did not have any effect on the total $K_v10.1$ content (siRNA mediated knockdown: $105 \pm 5\%$ of the control, overexpression: $97 \pm 5\%$ of control; Fig. 8*C*), indicating that, like in oocytes, CTTN does not affect the expression levels of $K_v10.1$.

Selective labeling and detection of membrane-bound $K_v10.1$ -BBS can be achieved by incubating living cells with the conjugate at room temperature for a short time to avoid internalization (19). Comparable with the findings in oocytes, overexpression of CTTN did not increase the membrane fraction of $K_v10.1$ -BBS ($112 \pm 21\%$ of control), whereas siRNA-mediated knockdown of CTTN (to $\sim 50\%$, as determined for every individual experiment) significantly reduced surface levels of $K_v10.1$ -BBS ($57 \pm 5\%$ of the control, Fig. 8*C*). Taken together, these results point to a CTTN-mediated regulation of $K_v10.1$ surface expression.

CTTN Stabilizes $K_v10.1$ at the Cell Membrane—As the amount of total $K_v10.1$ does not change in response to alterations in CTTN expression, two mechanisms to vary $K_v10.1$ membrane expression are conceivable. If CTTN is involved in trafficking processes of $K_v10.1$ toward the membrane, less $K_v10.1$ may reach the membrane when CTTN is missing. Alternatively, in the absence of CTTN, $K_v10.1$ that had reached the membrane would remain there for a shorter time, thus reducing the steady-state level.

If a trafficking process is involved, one would expect that depletion of CTTN prior to $K_v10.1$ expression would reduce the membrane expression of $K_v10.1$. To test this, sequential injection of the PTO and $K_v10.1$ cRNA was therefore performed in *Xenopus* oocytes. When $K_v10.1$ cRNA was injected 24 h before CTTN levels were lowered by PTO, $K_v10.1$ -mediated currents were significantly reduced to $51 \pm 11\%$ of control

Cortactin Controls $K_v10.1$ Functional Expression

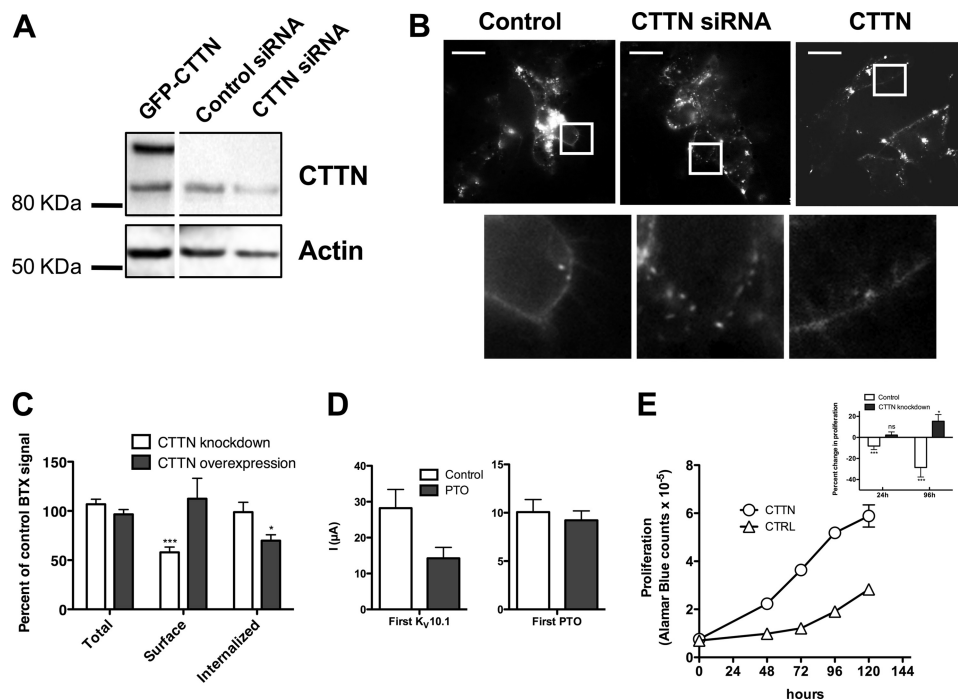


FIGURE 8. Effect of altered CTTN expression on $K_v10.1$ in HEK 293 cells stably expressing $K_v10.1$ -BBS. *A*, CTTN levels were influenced by either overexpression of a CFP-CTTN fusion protein or knockdown of CTTN by using siRNA as verified by immunoblotting against CTTN in HEK 293 cells stably expressing $K_v10.1$ -BBS. *B*, surface $K_v10.1$ -BBS labeled with a BTX-Alexa 555 conjugate was rarely observed in cells treated with siRNA against CTTN, whereas it was clearly seen in control cells (*control*) as well as in CFP-CTTN overexpressing cells (*CTTN*). Wide field microscopy on living cells, scale bars, 10 μ m. The areas indicated by a white square are shown at a higher magnification on the lower panel. *C*, quantification of surface $K_v10.1$ -BBS by ELISA revealed a clear reduction in response to CTTN depletion, whereas overexpression of CTTN did not change the amount of membrane-bound $K_v10.1$ -BBS significantly. Whole cell expression levels of $K_v10.1$ -BBS were independent of the modulated CTTN levels. To measure internalized $K_v10.1$ -BBS, cells were incubated with BTX-biotin for 1 h at physiological temperature to allow internalization. Subsequently, membrane labeling was removed by an acid wash. Overexpression of CTTN reduced internalized $K_v10.1$ -BBS in the given time, whereas depletion of CTTN did not have an effect. *D*, reduction of $K_v10.1$ current amplitude in *Xenopus* oocytes was only observed when CTTN depletion was achieved when PTO was injected before or simultaneously with $K_v10.1$, but not if it was injected 24 h later. *E*, growth of HeLa cells was stimulated by CTTN transfection (*circles*) as compared with transfection with empty vector (*triangles*). The inset shows that knockdown of $K_v10.1$ does not impair proliferation of CTTN-overexpressing cells.

levels (Fig. 8D). In contrast, when PTO injection was performed before $K_v10.1$ injection, there was no reduction of the $K_v10.1$ current with respect to the control ($92 \pm 9\%$ (Fig. 8D)). This observation argues against involvement of CTTN in trafficking processes, but instead indicates a role in stabilizing $K_v10.1$ at the plasma membrane.

We therefore tested internalization processes in mammalian cells using ELISA experiments similar to those described previously. Living HEK293 cells stably expressing $K_v10.1$ -BBS were incubated with a BTX-biotin conjugate for 1 h at physiological temperature to allow internalization of labeled $K_v10.1$ -BBS. Non-internalized BTX was then removed by acid wash. Quantification revealed that although $K_v10.1$ was clearly reduced at the membrane in response to CTTN depletion, the amount of internalized $K_v10.1$ within 1 h was not changed ($98 \pm 9\%$ of the control, Fig. 8C). CTTN overexpression on the other hand reduced the amount of $K_v10.1$ internalized in this time ($70 \pm 6\%$ of the control, Fig. 8C). These data are compatible with the proposed involvement of CTTN in stabilizing $K_v10.1$ in the plasma membrane. We therefore conclude that CTTN is probably involved in processes stabilizing the presence of $K_v10.1$ at the membrane.

If more $K_v10.1$ is available at the plasma membrane, the downstream effects of channel expression could also be enhanced. To test if this is the case, we overexpressed CTTN in HeLa cells, which have a relatively high endogenous expression

of $K_v10.1$. Channel knockdown in HeLa cells strongly reduces proliferation, indicating that the channel plays a role in this process. Transient transfection with CTTN increased proliferation rates of HeLa cells (Fig. 8E). Additionally, when a stable cell line overexpressing CTTN (by $\sim 25\%$ at the protein level, as estimated by Western blot and densitometry) was treated with siRNA against $K_v10.1$ (31), proliferation was not reduced (*inset* in Fig. 8E). These observations are compatible with enhanced levels of $K_v10.1$ at the cell surface in the presence of excess CTTN.

DISCUSSION

In this study we report that CTTN is an interaction partner of the voltage-gated potassium channel $K_v10.1$. Our results indicate that this interaction is direct as precipitation with purified proteins did not require the addition of any bridging factor. Different pulldown assay formats allowed us to identify the proline-rich region of CTTN as responsible for binding to $K_v10.1$. This region appears to be a major substrate for post-translational modifications in CTTN, bearing several well known phosphorylation sites. We have not examined possible post-translational regulation of the CTTN interaction with $K_v10.1$ and this does represent an area for further work.

We also observed co-localization of CTTN with $K_v10.1$ *in vivo* and in *Xenopus* oocytes we identified CTTN expression as a requirement for the $K_v10.1$ current, as complete depletion of

CTTN abolished current responses. The abundance of CTTN, however, does not appear to be a limiting factor for $K_V10.1$ functional expression, as overexpression of CTTN could not further enhance current amplitudes in oocytes, but it did accelerate proliferation of HeLa cells, a phenomenon that has been related to $K_V10.1$ expression (31). This effect is specific for $K_V10.1$, because its closest relative, $K_V10.2$, did not co-localize with CTTN *in vivo*, nor is $K_V10.2$ -mediated current affected by CTTN knockdown.

The known role of CTTN in actin cytoskeleton rearrangements (reviewed in Ref. 1) is unlikely to be responsible for its effects on $K_V10.1$ reported here; the effect was highly specific and did not apply to $K_V10.2$ -mediated current. In addition, interference with actin cytoskeleton rearrangement through Arp2/3 inhibition did not mimic the effect of CTTN knockdown.

Exchanging the C termini of $K_V10.1$ and $K_V10.2$ transferred the regulatory effect of CTTN to the latter, indicating that the specific functional interaction depends on the C terminus of $K_V10.1$. Deletion of residues 705–755 mimics the effects of CTTN depletion on $K_V10.1$, indicating that this segment is implicated in the interaction with CTTN. Chen and co-workers (32) examined truncation mutants of $K_V10.1$ and found that several deletions removing the tetramerizing coiled-coil at the distal C terminus of the channel (29) did show functional expression of currents. Interestingly, mutations deleting the domain identified here as the CTTN-interacting domain always produced non-functional channels. More recently (33), a crystal structure of the proximal C-domain and the putative cyclic nucleotide binding domain (*i.e.* the protein domain spanning between the last transmembrane segment S6 and the end of the CNBD) of a $K_V10.1$ family member revealed that it is able to form dimers, and that it would therefore potentially be implicated in the formation of multimeric channels. Our $\Delta 8$ construct (deletion of the TCC) failed to produce any currents, but apparently did generate proteins able to reach the membrane (see Fig. 5C) because we could detect internalized BTX in cells expressing this mutant. Additionally, the N terminus of the protein has also been implicated in tetramerization (34) in K_V11 channels. Altogether, these observations point to a scenario where the multimeric assembly occurs co-translationally with multiple interaction domains (N terminus, S6, proximal domain, and finally TCC “locking” and stabilizing the mature structure). The mature protein is then targeted to the plasma membrane and CTTN would stabilize it there. Nevertheless, residues 705–755 are probably not the only determinants of interaction with CTTN, because we still observed binding of the HP region to the deletion mutant as well as a residual effect on current amplitudes by CTTN depletion in *Xenopus* oocytes, pointing toward additional requirements for CTTN interaction.

CTTN can direct $K_V10.1$ to focal adhesions. These structures play a role in cancer via signaling cascades involving integrins as well as the FAK, a non-receptor tyrosine kinase mainly restricted to focal adhesions. These proteins seem to be key regulators in cancer progression (reviewed in Ref. 35). Again, a close relative of $K_V10.1$, HERG, ($K_V11.1$) is directly linked to $\beta 1$ integrin signaling pathways, where it modulates downstream

signaling elicited by integrin activation (36–38). $K_V10.1$, in addition to its presence at focal adhesions shown here seems to adopt a function in adhesion processes: its expression clearly influences adhesion of cells and the extracellular matrix is also able to modulate the $K_V10.1$ -mediated current, although a direct interaction with $\beta 1$ integrin has not been shown (39). The strong association of $K_V10.1$ with the actin cytoskeleton (39) might explain this behavior, and CTTN could serve to modulate interaction.

Other ion channels such as $K_V1.2$ and the large conductance calcium- and voltage-activated potassium channel $K_{Ca}1.1$ have been reported to bind to and to be influenced by CTTN via effects on affecting membrane expression or changes in open probability, respectively (4–8). In the latter, CTTN was suggested to bridge $K_{Ca}1.1$ channels to actin filaments, a process dependent on the phosphorylation state of CTTN and linkage of $K_{Ca}1.1$ channels to intracellular signaling (6, 7). $K_V10.1$ has been shown to be associated with actin fibers in CHO cells (39) and the $K_V10.1$ -mediated current is influenced by interactions with the cytoskeleton as disruption of the actin cytoskeleton by cytochalasin B dramatically increases $K_V10.1$ current density (15).

In our study, examination of the biophysical properties of $K_V10.1$ revealed that CTTN expression levels do not influence the single channel conductance or the open probability of this channel. Together with the fact that CTTN depletion clearly reduced membrane-located $K_V10.1$ in *Xenopus* oocytes as well as in HEK 293 cells stably expressing $K_V10.1$ -BBS, we conclude that CTTN has a regulatory effect on channel synthesis, maintenance, or transport. As CTTN depletion resulted in no detectable change in the amount of total whole cell $K_V10.1$, it is unlikely that CTTN affects channel synthesis or degradation. Sequential injection in *Xenopus* oocytes of $K_V10.1$ and the PTO affecting CTTN suggests that $K_V10.1$ transport toward the membrane is not affected by CTTN depletion. In line with this, the same amount of $K_V10.1$ -BBS seems to reach the membrane in a given time span in ELISA experiments on CTTN-depleted HEK 293 cells. Therefore, we propose that CTTN is involved in $K_V10.1$ endocytotic processes or in their regulation.

Consistent with this hypothesis, CTTN depletion is known to reduce endocytosis over clathrin-coated pits (35, 40, 41). However, in our system, CTTN depletion affects $K_V10.1$ surface expression, leading to clearly reduced membrane-resident protein. A similar effect is reported for $K_V1.2$ and interpreted to be the result of stabilization of the channel at the membrane as well as favoring its endocytosis in a phosphorylation-dependent manner (8). As the amount of internalized $K_V10.1$ is not altered by depletion of CTTN, but overexpression of CTTN does reduce the amount of internalized $K_V10.1$, we believe that CTTN plays a minor role in events of $K_V10.1$ internalization under basal conditions. Instead, we postulate a model whereby CTTN stabilizes $K_V10.1$ at the membrane; in the absence of CTTN, this would lead to a reduced membrane-residency time of $K_V10.1$ via faster internalization. Mechanistically, CTTN may connect $K_V10.1$ to the cytoskeleton by directing and stabilizing it at the desired locations and its ability to bind and induce polymerization of actin (reviewed by Ref. 4).

Cortactin Controls $K_v10.1$ Functional Expression

Additionally, CTTN has been linked to angiotensin II-induced tissue repair in smooth muscle cells, influencing proliferation and migration in an insulin-like growth factor-1 receptor and Src dependent way (42). Within this process, CTTN is phosphorylated and subsequently translocated to the membrane, especially to focal adhesions. The $K_v10.1$ -mediated current has been reported to be up-regulated in MCF-7 cells following stimulation with insulin-like growth factor-1 (13), and the pro-proliferative effects of this growth factor are dependent on $K_v10.1$. $K_v10.1$ overexpression alone has also been reported to increase proliferation rates (9); this increase requires functional ion channels at the plasma membrane because blockade by an extracellular antibody reduced this effect (43), but does not depend strictly on potassium permeation, because a point mutant unable to permeate K^+ recapitulates many of the effects of wild-type $K_v10.1$, although less efficiently (44). In good agreement with these observations, we found that overexpression of CTTN in HeLa cells increased proliferation, and rendered the cells no longer sensitive to $K_v10.1$ knockdown.

Overall, our observations would be compatible with a model where signaling pathways such as insulin-like growth factor-1R/Akt or Src induce CTTN-mediated alteration of $K_v10.1$ expression at the cell surface. In this way CTTN activity could be translated into cell cycle progression. Further work will be necessary to determine whether this is the case.

Acknowledgments—We thank Prof. Nils Brose for the gift of the cDNA library used in the yeast two-hybrid screen. We thank Victor Diaz, Sabine Klöppner, Tanja Nilsson, and Annett Sporning for excellent technical support.

REFERENCES

1. Ammer, A. G., and Weed, S. A. (2008) Cortactin branches out. Roles in regulating protrusive actin dynamics. *Cell. Motil. Cytoskeleton* **65**, 687–707
2. Weaver, A. M., Heuser, J. E., Karginov, A. V., Lee, W. L., Parsons, J. T., and Cooper, J. A. (2002) Interaction of cortactin and N-WASp with Arp2/3 complex. *Curr. Biol.* **12**, 1270–1278
3. Weed, S. A., Karginov, A. V., Schafer, D. A., Weaver, A. M., Kinley, A. W., Cooper, J. A., and Parsons, J. T. (2000) Cortactin localization to sites of actin assembly in lamellipodia requires interactions with F-actin and the Arp2/3 complex. *J. Cell Biol.* **151**, 29–40
4. Lua, B. L., and Low, B. C. (2005) Cortactin phosphorylation as a switch for actin cytoskeletal network and cell dynamics control. *FEBS Lett.* **579**, 577–585
5. Hattan, D., Nesti, E., Cachero, T. G., and Morielli, A. D. (2002) Tyrosine phosphorylation of Kv1.2 modulates its interaction with the actin-binding protein cortactin. *J. Biol. Chem.* **277**, 38596–38606
6. Tian, L., Chen, L., McClafferty, H., Sailer, C. A., Ruth, P., Knaus, H. G., and Shipston, M. J. (2006) A noncanonical SH3 domain binding motif links BK channels to the actin cytoskeleton via the SH3 adapter cortactin. *FASEB J.* **20**, 2588–2590
7. Tian, L., McClafferty, H., Chen, L., and Shipston, M. J. (2008) Reversible tyrosine protein phosphorylation regulates large conductance voltage- and calcium-activated potassium channels via cortactin. *J. Biol. Chem.* **283**, 3067–3076
8. Williams, M. R., Markey, J. C., Doczi, M. A., and Morielli, A. D. (2007) An essential role for cortactin in the modulation of the potassium channel Kv1.2. *Proc. Natl. Acad. Sci. U.S.A.* **104**, 17412–17417
9. Pardo, L. A., del Camino, D., Sánchez, A., Alves, F., Brüggemann, A., Beckh, S., and Stühmer, W. (1999) Oncogenic potential of EAG K^+ channels. *EMBO J.* **18**, 5540–5547
10. Wulff, H., Castle, N. A., and Pardo, L. A. (2009) Voltage-gated potassium channels as therapeutic targets. *Nat. Rev. Drug Discov.* **8**, 982–1001
11. Lin, H., Li, Z., Chen, C., Luo, X., Xiao, J., Dong, D., Lu, Y., Yang, B., and Wang, Z. (2011) Transcriptional and post-transcriptional mechanisms for oncogenic overexpression of ether α go-go K^+ channel. *PLoS ONE* **6**, e20362
12. Ouadid-Ahidouch, H., Le Bourhis, X., Roudbaraki, M., Toillon, R. A., Delcourt, P., and Prevarskaya, N. (2001) Changes in the K^+ current-density of MCF-7 cells during progression through the cell cycle. Possible involvement of a h-ether- α -gogo K^+ channel. *Recept. Channels* **7**, 345–356
13. Borowiec, A. S., Hague, F., Harir, N., Guénin, S., Guerneau, F., Gouilleux, F., Roudbaraki, M., Lassoued, K., and Ouadid-Ahidouch, H. (2007) IGF-1 activates hEAG K^+ channels through an Akt-dependent signaling pathway in breast cancer cells. Role in cell proliferation. *J. Cell. Physiol.* **212**, 690–701
14. Pardo, L. A., Brüggemann, A., Camacho, J., and Stühmer, W. (1998) Cell cycle-related changes in the conducting properties of r-eag K^+ channels. *J. Cell Biol.* **143**, 767–775
15. Camacho, J., Sánchez, A., Stühmer, W., and Pardo, L. A. (2000) Cytoskeletal interactions determine the electrophysiological properties of human EAG potassium channels. *Pflügers Arch. Eur. J. Physiol.* **441**, 167–174
16. Schuurin, E., Verhoeven, E., Mooi, W. J., and Michalides, R. J. (1992) Identification and cloning of two overexpressed genes, U21B31/PRAD1 and EMS1, within the amplified chromosome 11q13 region in human carcinomas. *Oncogene* **7**, 355–361
17. Weaver, A. M. (2008) Cortactin in tumor invasiveness. *Cancer Lett.* **265**, 157–166
18. Vojtek, A. B., Hollenberg, S. M., and Cooper, J. A. (1993) Mammalian Ras interacts directly with the serine/threonine kinase Raf. *Cell* **74**, 205–214
19. Kohl, T., Lörinczi, E., Pardo, L. A., and Stühmer, W. (2011) Rapid internalization of the oncogenic K^+ channel KV10.1. *PLoS ONE* **6**, e26329
20. Agarwal, J. R., Griesinger, F., Stühmer, W., and Pardo, L. A. (2010) The potassium channel Ether α go-go is a novel prognostic factor with functional relevance in acute myeloid leukemia. *Mol. Cancer* **9**, 18
21. Hemmerlein, B., Weseloh, R. M., Mello de Queiroz, F., Knötgen, H., Sánchez, A., Rubio, M. E., Martin, S., Schliephacke, T., Jenke, M., Heinz-Joachim-Radzun, Stühmer, W., and Pardo, L. A. (2006) Overexpression of Eag1 potassium channels in clinical tumours. *Mol. Cancer* **5**, 41
22. Stühmer, W. (1998) Electrophysiologic recordings from *Xenopus* oocytes. *Methods Enzymol.* **293**, 280–300
23. Heinemann, S. H., and Conti, F. (1992) Nonstationary noise analysis and application to patch clamp recordings. *Methods Enzymol.* **207**, 131–148
24. Ludwig, J., Terlau, H., Wunder, F., Brüggemann, A., Pardo, L. A., Marquardt, A., Stühmer, W., and Pongs, O. (1994) Functional expression of a rat homologue of the voltage-gated ether α go-go potassium channel reveals differences in selectivity and activation kinetics in the *Drosophila* channel and its mammalian counterpart. *EMBO J.* **13**, 4451–4458
25. Nolen, B. J., Tomasevic, N., Russell, A., Pierce, D. W., Jia, Z., McCormick, C. D., Hartman, J., Sakowicz, R., and Pollard, T. D. (2009) Characterization of two classes of small molecule inhibitors of Arp2/3 complex. *Nature* **460**, 1031–1034
26. Ludwig, J., Weseloh, R., Karschin, C., Liu, Q., Netzer, R., Engeland, B., Stansfeld, C., and Pongs, O. (2000) Cloning and functional expression of rat eag2, a new member of the ether- α -go-go family of potassium channels and comparison of its distribution with that of eag1. *Mol. Cell. Neurosci.* **16**, 59–70
27. Ju, M., and Wray, D. (2002) Molecular identification and characterization of the human eag2 potassium channel. *FEBS Lett.* **524**, 204–210
28. Schönherr, R., Gessner, G., Löber, K., and Heinemann, S. H. (2002) Functional distinction of human EAG1 and EAG2 potassium channels. *FEBS Lett.* **514**, 204–208
29. Jenke, M., Sánchez, A., Monje, F., Stühmer, W., Weseloh, R. M., and Pardo, L. A. (2003) C-terminal domains implicated in the functional surface expression of potassium channels. *EMBO J.* **22**, 395–403
30. Cao, H., Chen, J., Krueger, E. W., and McNiven, M. A. (2010) SRC-mediated phosphorylation of dynamin and cortactin regulates the “constitutive” endocytosis of transferrin. *Mol. Cell. Biol.* **30**, 781–792
31. Weber, C., Mello de Queiroz, F., Downie, B., Sukow, A., Stühmer, W., and

- Pardo, L. A. (2006) Silencing the activity and proliferative properties of the human Eag1 potassium channel by RNAi. *J. Biol. Chem.* **281**, 13030–13037
32. Chen, I. H., Hu, J. H., Jow, G. M., Chuang, C. C., Lee, T. T., Liu, D. C., and Jeng, C. J. (2011) Distal end of carboxyl terminus is not essential for the assembly of rat Eag1 potassium channels. *J. Biol. Chem.* **286**, 27183–27196
33. Brelidze, T. I., Carlson, A. E., Sankaran, B., and Zagotta, W. N. (2012) Structure of the carboxyl-terminal region of a KCNH channel. *Nature* **481**, 530–533
34. Phartiyal, P., Jones, E. M., and Robertson, G. A. (2007) Heteromeric assembly of human ether-à-go-go-related gene (hERG) 1a/1b channels occurs cotranslationally via N-terminal interactions. *J. Biol. Chem.* **282**, 9874–9882
35. Luo, M., and Guan, J. L. (2010) Focal adhesion kinase: a prominent determinant in breast cancer initiation, progression and metastasis. *Cancer Lett.* **289**, 127–139
36. Arcangeli, A., Becchetti, A., Cherubini, A., Crociani, O., Defilippi, P., Guasti, L., Hofmann, G., Pillozzi, S., Olivotto, M., and Wanke, E. (2004) Physical and functional interaction between integrins and hERG potassium channels. *Biochem. Soc. Trans.* **32**, 826–827
37. Cherubini, A., Hofmann, G., Pillozzi, S., Guasti, L., Crociani, O., Cilia, E., Di Stefano, P., Degani, S., Balzi, M., Olivotto, M., Wanke, E., Becchetti, A., Defilippi, P., Wymore, R., and Arcangeli, A. (2005) Human ether-a-go-go-related gene 1 channels are physically linked to $\beta 1$ integrins and modulate adhesion-dependent signaling. *Mol. Biol. Cell* **16**, 2972–2983
38. Hofmann, G., Bernabei, P. A., Crociani, O., Cherubini, A., Guasti, L., Pillozzi, S., Lastraioli, E., Polvani, S., Bartolozzi, B., Solazzo, V., Gragnani, L., Defilippi, P., Rosati, B., Wanke, E., Olivotto, M., and Arcangeli, A. (2001) HERG K^+ channels activation during β_1 integrin-mediated adhesion to fibronectin induces an up-regulation of $\alpha_v\beta_3$ integrin in the preosteoclastic leukemia cell line FLG 29.1. *J. Biol. Chem.* **276**, 4923–4931
39. Toral, C., Mendoza-Garrido, M. E., Azorín, E., Hernández-Gallegos, E., Gomora, J. C., Delgadillo, D. M., Solano-Agama, C., and Camacho, J. (2007) Effect of extracellular matrix on adhesion, viability, actin cytoskeleton, and K^+ currents of cells expressing human ether a go-go channels. *Life Sci.* **81**, 255–265
40. Cao, H., Orth, J. D., Chen, J., Weller, S. G., Heuser, J. E., and McNiven, M. A. (2003) Cortactin is a component of clathrin-coated pits and participates in receptor-mediated endocytosis. *Mol. Cell. Biol.* **23**, 2162–2170
41. Chen, L., Wang, Z. W., Zhu, J. W., and Zhan, X. (2006) Roles of cortactin, an actin polymerization mediator, in cell endocytosis. *Acta Biochim. Biophys. Sin.* **38**, 95–103
42. Zahradka, P., Storie, B., and Wright, B. (2009) IGF-1 receptor transactivation mediates Src-dependent cortactin phosphorylation in response to angiotensin II. *Can. J. Physiol. Pharmacol.* **87**, 805–812
43. Gómez-Varela, D., Zwick-Wallasch, E., Knötgen, H., Sánchez, A., Hettmann, T., Ossipov, D., Weseloh, R., Contreras-Jurado, C., Rothe, M., Stühmer, W., and Pardo, L. A. (2007) Monoclonal antibody blockade of the human Eag1 potassium channel function exerts antitumor activity. *Cancer Res.* **67**, 7343–7349
44. Downie, B. R., Sánchez, A., Knötgen, H., Contreras-Jurado, C., Gymnopoulos, M., Weber, C., Stühmer, W., and Pardo, L. A. (2008) Eag1 expression interferes with hypoxia homeostasis and induces angiogenesis in tumors. *J. Biol. Chem.* **283**, 36234–36240